Title

A study of temperature dependent current–voltage (I–V–T) characteristics in Ni/sol–gel β-Ga2O3/n-GaN structure

Journal

Journal of Materials Science: Materials in Electronics, 29(13)

ISSN

0957-4522

Authors

Gao, Jianyi
Kaya, Ahmet
Chopdekar, Rajesh V
et al.

Publication Date

2018-07-01

DOI

10.1007/s10854-018-9213-y

Peer reviewed

Journal of Materials Science: Materials in Electronics
https://doi.org/10.1007/s10854-018-9213-y

A study of temperature dependent current–voltage (I–V–T) characteristics in Ni/sol–gel β-Ga_2O_3/n-GaN structure

Jianyi Gao[1] · Ahmet Kaya[1] · Rajesh V. Chopdekar[2] · Zheng Xu[1] · Yayoi Takamura[2] · M. Saif Islam[1] · Srabanti Chowdhury[1]

Received: 23 February 2018 / Accepted: 30 April 2018

Abstract
β-Ga_2O_3 thin films were grown on n-type GaN substrates using the sol–gel method. The forward-biased temperature dependent current–voltage (I–V–T) characteristics of Ni/β-Ga_2O_3/GaN structure have been investigated in the temperature range of 298–473 K. The apparent barrier height (ϕ_{ap}) increased while the ideality factor (n) decreased with the increase in temperature. Such a temperature dependent behavior of ϕ_{ap} and n was explained by the inhomogeneity of ϕ_{ap}, which obeyed Gaussian distribution with zero-bias mean barrier height ($\bar{\phi}_{B0}$) of 1.02 ± 0.02 eV and standard deviation (σ_{s0}) of 153 ± 0.04 mV. Subsequently, $\bar{\phi}_{B0}$ and Richardson constant A^* were obtained from the slope and intercept of the modified Richardson plot as 0.99 ± 0.01 e V and 67.2 A cm^{-2} K^{-2}, respectively. The $\bar{\phi}_{B0}$ obtained from the modified Richardson plot was in good agreement with the theoretical value calculated from the work function of Ni and electron affinity of β-Ga_2O_3. The I–V–T characteristics of Ni/β-Ga_2O_3/GaN MOS structures can be successfully explained by the thermionic emission theory with a single Gaussian distribution of the barrier height.

1 Introduction

Gallium nitride (GaN) has been extensively investigated in optoelectronics as it can realize high performance LED combing with other materials such as ZnO [1] and $CsPbBr_3$ [2]. Recently, GaN high-electron-mobility-transistors (HEMTs) have gained considerable attention for power switching applications due to its high-speed switching performance as well as high breakdown voltage [3]. Metal-oxide-semiconductor (MOS) structures are commonly adopted as gate control terminal in GaN HEMTs. In recent years, gallium oxide (Ga_2O_3) has drawn increasing attention as a dielectric material owing to its superior dielectric properties such as high dielectric constant (9.9–10.2) [4], high breakdown strength (> 7 MV cm^{-1}) [5], and high chemical and thermal stability. Ga_2O_3 thin-films were successfully obtained on various foreign substrates using various techniques such as sputtering [6], atomic layer deposition [7, 8], and oxidation [9, 10]. Ga_2O_3/GaN MOS structures are of particular interest due to the fact that a few monolayers of native Ga_2O_3 decorate the GaN surface because of the spontaneous termination of the Ga-atoms with oxygen [11, 12], affecting the interface property between the oxide and underlying GaN. The effect of the presence of Ga_2O_3 layer on the MOS structures has been studied by intentionally growing Ga_2O_3 layer on GaN. For example, Lee et al. grew a Ga_2O_3 layer on n-type GaN using a photoelectrochemical method involving a He–Cd laser and estimated interface-state density (D_{it}) of 2.53×10^{11} cm^{-2} eV^{-1} [13]. Yamada et al. characterized D_{it} of thermal oxidized GaO_x on GaN to be 1.7×10^{11} cm^{-2} eV^{-1} [6]. These studies indicated the intrinsically superior nature of the Ga_2O_3/GaN interfaces, inspired by thermal oxidized SiO_2 with Si that is commonly adopted in silicon CMOS technology.

Recent studies have pointed out insufficient conduction band offset (ΔE_C) at the Ga_2O_3/GaN interfaces. Grodzicki et al. used oxygen bombardment to oxidize GaN and measured ΔE_C of Ga_2O_3 and GaN to be 0.35 eV using X-ray photoelectron spectroscopy [14]. Wei et al. measured ΔE_C of thermal oxidation grown Ga_2O_3 and GaN to be 0.1 ± 0.08 eV [15]. Conduction mechanism of n-type MOS structures with low ΔE_C is more likely to be dominated by thermionic emission (TE), as electrons easily overcome the potential barrier

✉ Jianyi Gao
jiagao@ucdavis.edu

[1] Department of Electrical and Computer Engineering, University of California, Davis, CA, USA

[2] Department of Materials Science and Engineering, University of California, Davis, CA, USA

Published online: 04 May 2018

at oxide/semiconductor interfaces and reach the metal side. The current–voltage characteristics of such MOS structures become similar to those of metal-semiconductor (MS) type diodes. In addition, Fowler–Nordheim tunneling current is more pronounced at high electric field when ΔE_C is sufficiently low. These facts can result in large gate leakage current when MOS structures are forward-biased, suggesting that Ga_2O_3 standalone may not be an appropriate gate oxide for GaN-based MOS structure.

Previously, we have successfully deposited β-Ga_2O_3 on GaN using a sol–gel process [16]. Sol–gel method has demonstrated to be a simple and inexpensive way of growing thin-film dielectrics on semiconductors [17, 18]. D_{it} and ΔE_C between sol–gel β-Ga_2O_3 and GaN were characterized to be 1.75×10^{12} cm^{-2} and 0.35 eV, respectively. Owing to insufficient ΔE_C, there was relatively high gate leakage current in the forward-bias. In an attempt to systematically investigate the electrical characteristics of β-Ga_2O_3/GaN MOS structures, temperature dependent current–voltage (I–V–T) measurement was performed in this study. Analysis of the I–V–T characteristics of the Ni/β-Ga_2O_3/GaN MOS structures not only gave detailed information about their conduction mechanism but also the effect of β-Ga_2O_3 on the device performance. The I–V–T characteristics revealed an increase in apparent barrier height (ϕ_{ap}) and a decrease in ideality factor (n) with an increase in temperature. There have been extensive studies about the temperature dependent behavior of ϕ_{ap} and n [19, 20]. Such behavior of ϕ_{ap} and n resulted from the inhomogeneity of ϕ_{ap} due to the presence of β-Ga_2O_3 interfacial layer and it was manifest as a deviation from linearity in the conventional Richardson plot. Zero-bias mean barrier height ($\bar{\phi}_{B0}$) and Richardson constant were extracted from the modified Richardson plot. The value of $\bar{\phi}_{B0}$ was in good agreement with its theoretical value. The I–V–T characteristics of Ni/β-Ga_2O_3/GaN MOS structures can be successfully explained by the TE theory with a single Gaussian distribution of the barrier height.

2 Sample preparation and structural properties

Sol–gel β-Ga_2O_3 was coated on a MOCVD-grown GaN-on-sapphire wafer consisting of 1 μm n-GaN layer with doping of ~ 1×10^{17} cm^{-3} on the top and 1 μm n^+ GaN layer with doping of ~ 3×10^{18} cm^{-3} on the bottom (see Fig. 2). Detailed description on the sol–gel β-Ga_2O_3 process can be found in our report [5, 16]. Structural characterization of the films was performed after the annealing step with a Bruker D8 Discover high-resolution X-ray diffraction (XRD) system equipped with a Cu K-alpha X-ray source. Measurements were performed in a grazing incidence angle of 0.8° to maximize diffracted intensity from the Ga_2O_3 film and minimize intensity from the GaN/sapphire substrate. Figure 1a shows a typical XRD pattern of the annealed Ga_2O_3 film with peaks indexed to monoclinic β-Ga_2O_3 (ICDD powder diffraction file 41-1103). The surface morphology of the β-Ga_2O_3 film was examined by atomic force microscopy (AFM) using an Asylum Research MFP-3D AFM tool as shown in Fig. 1b. The root-mean-square (RMS) roughness of 5 × 5 μm scan area of β-Ga_2O_3 surface is ~ 0.55 nm, which is closed to the RMS of GaN substrate surface, 0.57 nm. It implies that smooth β-Ga_2O_3 film was coated on GaN.

After the structural characterization of the films, MOS structures in Fig. 2 were fabricated with the following steps. First, mesa isolation was performed using buffered oxide etch (BOE) wet etching for β-Ga_2O_3, and subsequent Cl_2-based reactive-ion etching for GaN. Then, ohmic contacts consisting of Ti/Au (20/200 nm) was formed by e-beam evaporation and lift-off process on the etch-exposed n^+ GaN layer. Finally,

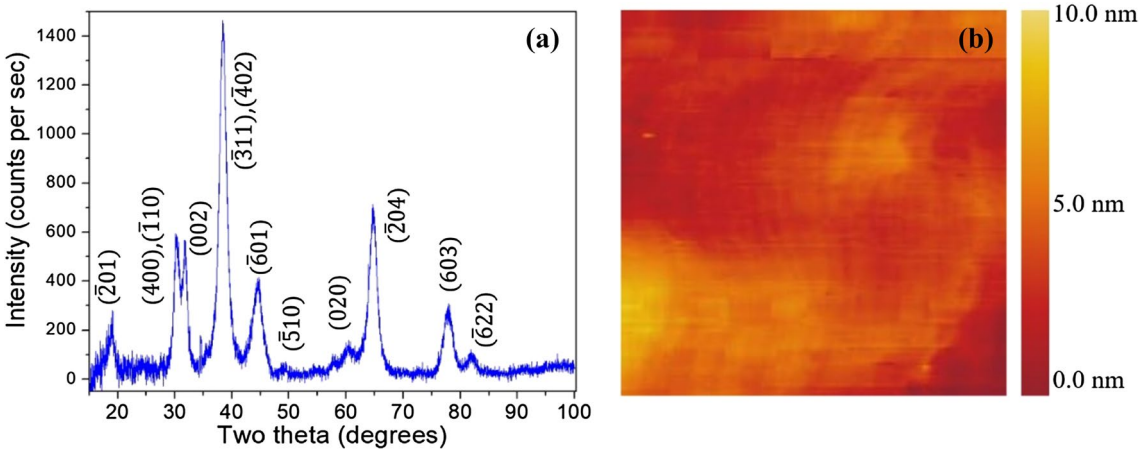

Fig. 1 **a** XRD pattern with peaks indexed to the β-Ga_2O_3 phase and **b** 5 × 5 μm AFM image of the sol–gel β-Ga_2O_3 film (RMS surface roughness = 0.55 nm)

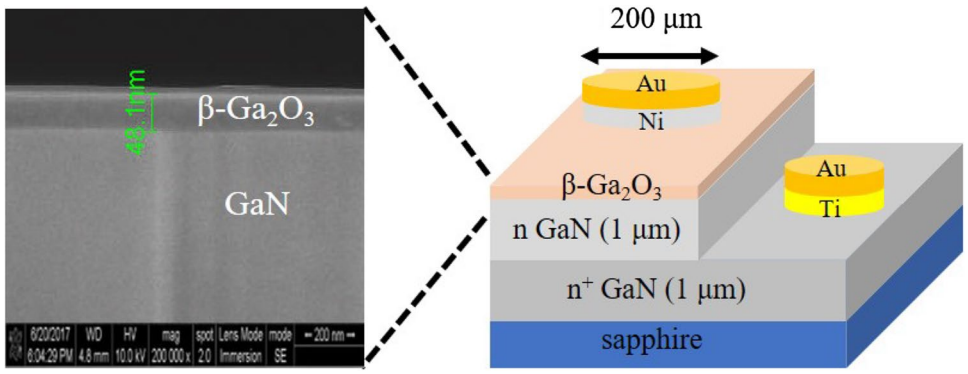

Fig. 2 Schematics of MOS diode and cross-sectional SEM image

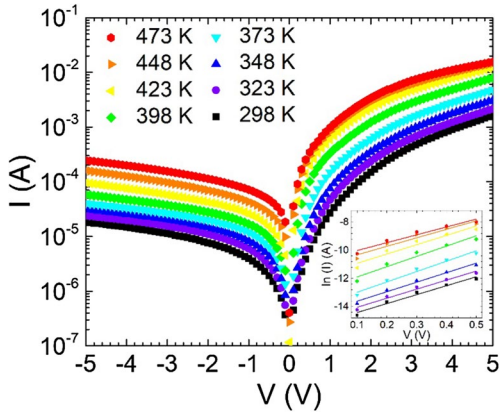

Fig. 3 Forward and reverse bias I–V–T characteristics of the Ni/β-Ga_2O_3/GaN MOS structure. The inset plots linear relationship of *lnI* versus *V* at low voltage

a gate contact consisting of Ni/Au (20/200 nm) was made on the β-Ga_2O_3 film. The β-Ga_2O_3 film thickness was determined to be 48.2 ± 2.3 nm from the cross-sectional scanning electron microscope (SEM) image on multiple locations. A Keithley 4200-SCS parameter analyzer was used to measure the I–V–T characteristics.

3 Results and discussion

Figure 3 shows the forward and reverse bias I–V–T characteristics of Ni/β-Ga_2O_3/GaN MOS structures in the temperature range of 298–473 K. For MOS structures with low ΔE_C between oxide and semiconductor, the conduction mechanism is governed by TE and I–V characteristics can be expressed by [21].

$$I = I_0\left[exp\left(\frac{q(V - IR_s)}{nkT}\right) - 1\right] \tag{1}$$

where n is the ideality factor IR_s is the voltage drop across R_s of structure, I_0 is the saturation current and can be extracted from the straight line intercept of *lnI–V* plot (Fig. 3 inset) at zero bias. I_0 is expressed by:

$$I_0 = AA^*T^2 \exp\left(-\frac{q\varphi_{ap}}{kT}\right) \tag{2}$$

where A is the diode area, ϕ_{ap} is the apparent or measured barrier height, A^* is the Richardson constant and equal to 26.4 A cm^{-2} K^{-2} for n-type GaN [22], respectively. The value of I_0 was obtained from the intercept of *lnI–V* plot for each temperature. Subsequently, using the I_0 and the value of A, the value of ϕ_{ap} was obtained from Eq. (2) for each temperature as:

$$\varphi_{ap} = \frac{kT}{q}\ln\left(\frac{AA^*T^2}{I_0}\right) \tag{3}$$

The other important diode parameter, ideality factor n was obtained from the slope of *lnI–V* plot for each temperature as

$$n = \frac{q}{kT}\frac{dV}{d(\ln I)} \tag{4}$$

The temperature dependent values of I_0, n and ϕ_{ap} were summarized in Table 1. The experimental values of I_0, n and ϕ_{ap} range from 2.89×10^{-7} A, 5.5 and 0.55 eV (at 298 K), and 2.56×10^{-5} A, 3.5 and 0.74 eV (at 473 K). Ideality factor

Table 1 The values of various electrical parameters in the temperature range of 298–473 K

T (K)	I_0 (A)	n	ϕ_{ap} (eV)
298	2.89×10^{-7}	5.5	0.55
323	4.17×10^{-7}	5.13	0.60
348	6.21×10^{-7}	4.84	0.63
373	1.10×10^{-6}	4.55	0.67
398	3.29×10^{-6}	4.29	0.68
423	9.29×10^{-6}	4.03	0.69
448	1.81×10^{-5}	3.84	0.71
473	2.56×10^{-5}	3.51	0.74

n decreased while ϕ_{ap} increased with an increase in temperature as shown in Fig. 4. Such a temperature dependent behavior of ϕ_{ap} and n is attributed to the inhomogeneity of the barrier height due to the presence of β-Ga_2O_3 thin film between the metal and GaN. At low temperature, electrons without sufficient energy can only surmount patches with lower Schottky barrier [23–25]. As the temperature increases, more and more electrons gain sufficient energy to overcome higher barrier, leading to the measurement of higher apparent Schottky barrier height. Tung pointed out a negative correlation between the apparent Schottky barrier and the ideality factor [26]. Therefore, the ideality factor decreases with the increase in temperature. Moreover, interface states can also cause such behavior of ϕ_{ap} and n [27]. The reverse bias current increases with the increase of temperature, which can be attributed to the tunneling through the surface and bulk traps [28–30]. This mechanism was proved based on greater-than-unity ideality factors extracted from the forward I–V–T plots.

Conventional Richardson plot or activation energy plot ($\ln\left(I_0/T^2\right)$ vs. $1/T$) has usually been adopted to evaluate the ϕ_{ap}. Figure 5 shows the conventional Richardson plot for Ni/β-Ga_2O_3/GaN structure. Richardson plot shows a poor linear fitting in the temperature range of 298–473 K, with the slope of − 2.93 and intercept of − 15.31. The activation energy (E_a) and A^* were extracted from the slope and intercept as 0.254 eV and 7.145×10^{-4} A cm^{-2} K^{-2}, respectively. This experimental value of A^* is significantly lower than the theoretical value of n-GaN (26.4 A cm^{-2} K^{-2}). Horvath et al. [31] explained the low value A^* may be due to the lateral inhomogeneity of the barrier height at M/S interface.

As discussed above, the increase in ϕ_{ap} and decrease in n with increasing temperature and low value A^* extracted from conventional Richardson plot in Fig. 5 were due to the lateral inhomogeneity of barrier height. The inhomogeneity can be described by a Gaussian distribution with a mean barrier

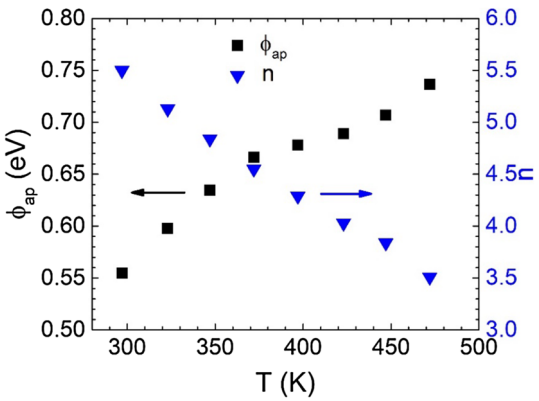

Fig. 4 Apparent barrier height (ϕ_{ap}) and ideality factor (n) as a function of temperature

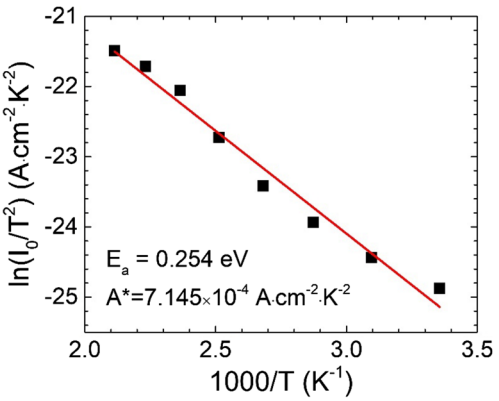

Fig. 5 Conventional Richardson plot for Ni/ β-Ga_2O_3/GaN MOS structure

height and a standard deviation. According to single Gaussian distribution theory, the ϕ_{ap} and the ideality factor can be expressed by the following relations: [32]

$$\varphi_{ap} = \overline{\varphi}_{B0} - \frac{q\sigma_{s0}^2}{2kT} \tag{5}$$

$$\frac{1}{n} - 1 = -\rho_2 - \frac{q\rho_3}{2kT} \tag{6}$$

where $\bar{\phi}_{B0}$ is the zero-bias mean barrier height, σ_{s0} is the zero-bias standard deviation of the barrier height distribution which is a measure of the barrier height homogeneity, ρ_2 and ρ_3 are the voltage deformation coefficients. The experimental ϕ_{ap} versus $q/2kT$ and $n^{-1} - 1$ versus $q/2kT$ plots are shown in Fig. 6. The values of $\bar{\phi}_{B0}$ and σ_{s0} obtained from the intercept and slope of ϕ_{ap} versus $q/2kT$ plot are 1.02 ± 0.02 eV and 153 ± 0.04 mV, respectively. The value of σ_{s0} indicates that

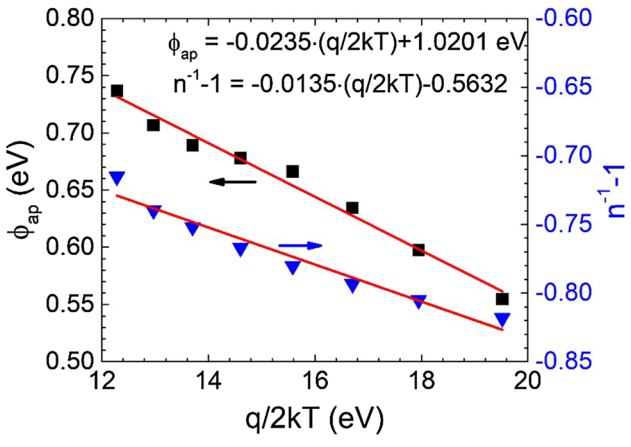

Fig. 6 Apparent barrier height and $n^{-1} - 1$ versus $q/2kT$ according to single Gaussian distribution of barrier height. The goodness of the linear fit is 0.980 and 0.946, respectively

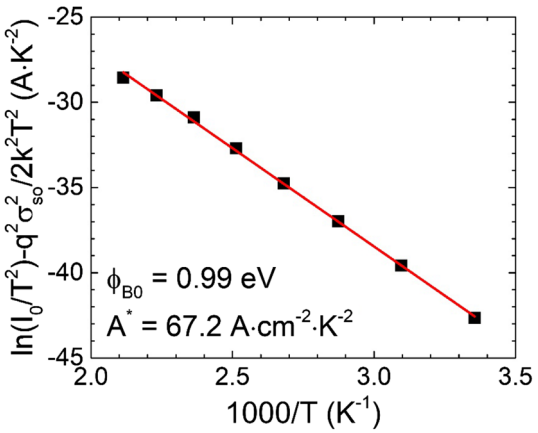

Fig. 7 Modified Richardson plot according to single Gaussian distribution of barrier height. The goodness of linear fit is 0.999

the existence of a distribution of barrier height or patches at around $\bar{\phi}_{B0}$. As can be seen in Table 1, the ϕ_{ap} calculated from the forward bias I–V is always smaller than $\bar{\phi}_{B0}$ for each temperature. The values of ρ_2 and ρ_3 obtained from the intercept and slope of $n^{-1}-1$ versus $q/2kT$ plot were 0.5632 and 0.0135 V, respectively.

The conventional activation energy $ln(I_0/T^2)$ versus $1/T$ plot should be linear in the ideal case and gives A^* and $\bar{\phi}_{B0}$ as intercept and slope calculations based on the TE current mechanism. For MOS structures with inhomogeneous barrier height, however, the goodness of linear fitting of conventional activation energy plot is poor (as shown in Fig. 5). When considering Eqs. (3) and (5), a modified activation energy expression according to the Gaussian distribution of the barrier heights can be rewritten as:

$$\ln\left(\frac{I_0}{T^2}\right)-\left(\frac{q^2\sigma_{s0}^2}{2k^2T^2}\right)=\ln\left(AA^*\right)-\frac{q\overline{\varphi}_{B0}}{kT} \tag{7}$$

Using the experimental I_0 data, the modified $\ln\left(I_0/T^2\right)-q^2\sigma_{s0}^2/2k^2T^2$ versus $1/T$ plot can be obtained according to Eq. (7). This plot should give a straight line with the slope yielding $\bar{\phi}_{B0}$ and the intercept at the ordinate yielding A^* for a given diode area A. Figure 7 represents the plot calculated with σ_{s0} obtained from Fig. 6 over the temperature range of 298–473 K. A good liner fit to the modified experimental data is depicted which represents the true activation energy plot. The slope yielded $\bar{\phi}_{B0}$ of 0.99 ± 0.01 eV, matching the $\bar{\phi}_{B0}$ value obtained from the ϕ_{ap} versus $1/T$ plot in Fig. 6. This result also matches the theoretical barrier height of 1.01 ± 0.05 eV, calculated from the difference in electron affinity of β-Ga_2O_3 ($=4.00\pm0.05$ eV) [33] and work function of Ni ($=5.01$ eV). The intercept at the ordinate gives the Richardson constant A^* of 67.2 A cm^{-2} K^{-2}. A good linear fitting in the modified Richardson plot indicates that the I–V–T characteristics of Ni/β-Ga_2O_3/GaN MOS structures can be explained by the TE theory with a single Gaussian distribution of the barrier height.

4 Conclusion

A detailed analysis of the I–V–T characteristics of the Ni/sol–gel β-Ga_2O_3/GaN MOS structures has been made to investigate the electrical characteristics of the MOS structures. Experimental results showed that the electrical parameters such as I_0, n, and ϕ_{ap} were in strong function of temperature, which was due to the lateral inhomogeneity of barrier height. In order to interpret such behavior of ϕ_{ap} and n, both the ϕ_{ap} versus $q/2kT$ and $(n^{-1}-1)$ vs $q/2kT$ plots were drawn to obtain an evidence of a Gaussian distribution of the barrier height. The $\bar{\phi}_{B0}$ and σ_{s0} obtained from the intercept and slope of ϕ_{ap} vs $q/2kT$ plot were 1.02 ± 0.02 eV and 153 ± 0.04 mV, respectively. Subsequently, the $\bar{\phi}_{B0}$ and A^* were obtained from the slope and intercept of the modified Richardson plot as 0.99 ± 0.01 e V and 67.2 A cm^{-2} K^{-2}. The $\bar{\phi}_{B0}$ obtained from both ϕ_{ap} versus $q/2kT$ plot and modified Richardson plot are in good agreement with the theoretical value calculated from the work function of Ni and electron affinity of β-Ga_2O_3. The I–V–T characteristics of Ni/β-Ga_2O_3/GaN MOS structures can be successfully explained by the TE theory with a single Gaussian distribution of the barrier height.

References

1. I.E. Titkov, L.A. Delimova, A.S. Zubrilov, N.V. Seredova, I.A. Liniichuk, I.V. Grekhov, J. Mod. Opt **56**, 653 (2009)
2. C. Li, Z. Zang, W. Chen, Z. Hu, X. Tang, W. Hu, K. Sun, X. Liu, W. Chen, Opt. Express **24**, 15071 (2016)
3. J. Gao, M. Hao, W. Li, Z. Xu, S. Mandal, R. Nemanich, S. Chowdhury, Phys. Status Solidi A **5**, 1700498 (2018)
4. M. Passlack, N.E.J. Hunt, E.F. Schubert, G.J. Zydzik, M. Hong, J.P. Mannaerts, R.L. Opila, R.J. Fischer, Appl. Phys. Lett. **64**, 2715 (1994)
5. A. Kaya, H. Mao, J. Gao, R.V. Chopdekar, Y. Takamura, S. Chowdhury, M.S. Islam, IEEE Trans. Electron Devices **64**, 2047 (2017)
6. T. Yamada, J. Ito, R. Asahara, K. Watanabe, M. Nozaki, T. Hosoi, T. Shimura, H. Watanabe, Appl. Phys. Lett. **110**, 261603 (2017)
7. D.J. Comstock, J.W. Elam, Chem. Mater. **24**, 4011 (2012)
8. R.K. Ramachandran, J. Dendooven, J. Botterman, S.P. Sree, D. Poelman, J.A. Martens, H. Poelmand, C. Detavernier, J. Mater. Chem. A **2**, 19232 (2014)
9. T. Hossain, D. Wei, N. Nepal, N.Y. Garces, J.K. Hite, H.M. Meyer III, C.R. Eddy Jr., T. Baker, A. Mayo, J. Schmitt, J.H. Edgar, Phys. Status Solidi C **11**, 565 (2014)
10. T. Yamada, J. Ito, R. Asahara, K. Watanabe, M. Nozaki, S. Nakazawa, Y. Anda, M. Ishida, T. Ueda, A. Yoshigoe, T. Hosoi, T. Shimura, H. Watanabe, J. Appl. Phys. **121**, 035303 (2017)

11. K.J. Chen, S. Yang, Z. Tang, S. Huang, Y. Lu, Q. Jiang, S. Liu, C. Liu, B. Li, Phys. Status Solidi A **5**, 1059 (2015)
12. K. Prabhakaran, T.G. Andersson, K. Nozawa, Appl. Phys. Lett. **69**, 3212 (1996)
13. C.-T. Lee, H.-W. Chen, H.-Y. Lee, Appl. Phys. Lett. **82**, 4304 (2003)
14. M. Grodzicki, P. Mazur, S. Zuber, J. Brona, A. Ciszewski, Appl. Surf. Sci. **304**, 20 (2014)
15. W. Wei, Z. Qin, S. Fan, K. Shi, Q. Zhu, G. Zhang, Nanoscale Res. Lett. **7**, 562 (2012)
16. J. Gao, A. Kaya, R.V. Chopdekar, D.M. Dryden, Y. Takamura, M.S. Islam, S. Chowdhury, 75th Annual Device Research Conference (DRC), South Bend, IN, 2017, pp. 1–2. (2017). https://doi.org/10.1109/DRC.2017.799944
17. A. Kumar, S. Mondal, K.S.R.K. Rao, J. Mater. Sci. **27**, 5264 (2016)
18. M.H. Amiri, N. Namdar, A. Mashayekhi, F. Ghasemi, Z. Sanaee, S. Mohajerzadeh, J. Nanopart. Res. **18**, 237 (2016)
19. R.T. Tung, Mater. Sci. Eng. R **35**, 1 (2001)
20. I. Afandiyeva, S. Demirezen, Ş Altındal, J. Alloy. Compd. **552**, 423 (2013)
21. S.M. Sze, *Physics of Semiconductor Devices*, 3 edn. (Wiley, Hoboken, 2007), p. 161
22. X.J. Wang, L. He, J. Electron. Mater. **27**, 1272 (1998)
23. S. Karatas, S. Altindal, A. Turut, A. Ozmen, Appl. Surf. Sci. **217**, 250 (2003)
24. J.H. Werner, H.H. Guttler, J. Appl. Phys. **69**, 152 (1991)
25. A. Gumus, A. Turut, N. Yalcin, J. Appl. Phys. **91**, 245 (2002)
26. R.T. Tung, Phys. Rev. B **45**, 13509 (1992)
27. B.P. Lakshmi, M.S.P. Reddy, A.A. Kumar, V.R. Reddy, Curr. Appl. Phys. **12**, 765 (2012)
28. E. Marıl, A. Kaya, S. Koçyiğit, Ş Altındal, Mater. Sci. Semicond. Process. **31**, 256 (2015)
29. S.K. Tripathi, M. Sharma, J. Appl. Phys. **111**, 074513 (2012)
30. S. Saadaoui, M.M.B. Salem, M. Gassoumi, H. Maaref, C. Gaquière, J. Appl. Phys. **110**, 013701 (2011)
31. Z.J. Horvath, J. Appl. Phys. **64**, 6780 (1988)
32. R.F. Schmisdorf, T.U. Kampen, W. Monch, Surf. Sci. **324**, 249 (1995)
33. M. Mohamed, K. Irmscher, C. Janowitz, Z. Galazka,2 R. Manzke, R. Fornari, Appl. Phys. Lett. **101**, 132106 (2012)